

Modeling and Optimization of an Obstacle Detection System for Small UAVs

Nuno Miguel Portal Alturas
nuno.alturas@tecnico.ulisboa.pt

Instituto Superior Técnico, Universidade de Lisboa, Portugal

January 2021

Abstract

In the last years, the unmanned aerial vehicles (UAV) market has expanded and diversified substantially. This work presents a solution for the enhancement of safety during the flight of small fixed-wing UAVs, regarding the detection of obstacles during flight. This task was achieved by making a market study on available sensors to find the most suitable to equip a UAV and by modeling them, so that these models could be integrated into collision detection and avoidance simulations. A study was also made on different tracking filters and sensor fusion techniques, where the Converted Measurement Kalman Filter and the Weighted Filter technique were found to be the best options to implement. In the performed simulations, the used avoidance method was the Potential Fields for being computationally inexpensive and for providing feasible solutions in real time. Several parametric studies were conducted to test the performance of the studied sensors and to see how different sensor parameters affect the success of the obstacle avoidance. In these tests, the characteristics of the sensors were deemed adequate for avoiding obstacles when integrated into small UAVs. An optimization study was also conducted, using a genetic algorithm, to find the orientation of sensors, for different sets of sensors, that results in the best performance in a collection of random generated scenarios. It is shown that, overall, the developed system provided a satisfactory solution.

Keywords: Potential Fields, Genetic Algorithm, Kalman Filter, Unbiased Conversion, Sensor Fusion

1. Introduction

Like many other technologies, Unmanned Aircraft Vehicles (UAVs) were initially developed for military purposes and have since made their way into the civil domain. Nowadays, UAV applications include but are not limited to commercial photography and video, precision agriculture, border control and delivery of goods. The market is still growing and projections show that non-military UAV production will total 14.3 billion dollars in 2028, while totaling 4.9 billion dollars in 2019 [1].

UAV classification is important to differentiate existing systems, since each category has different legal regulations, and also commercial and operational purposes. Considering the classification of UAVs proposed in reference [2], our work is specifically aimed at fixed-wing mini UAVs (maximum take-off weight < 25 kg, range < 10 km, endurance < 2 h and flight altitude < 120 m), due to the big share of the market that this category occupies and due to their versatility and low-cost. An example of a representative UAV, to which this work is aimed, is the AR4 (Figure 1), an autonomous, fixed-wing and mini UAV designed and manufactured by the Portuguese company Tekever. This aircraft has a

maximum take-off weight of 4 kg, an endurance of 2 hours, a maximum speed of 15 m/s and it is hand launched for take-off [3].



Figure 1: Tekever AR4 UAV [3]

For the UAVs to perform the functions previously described efficiently, autonomous and Beyond Visual Line of Sight (BVLOS) flight is essential, which is already foreseen by the Portuguese law. Furthermore, for an autonomous and BVLOS flight to be safe and effective, a reliable Sense and Avoidance (S&A) system is needed. There are already numerous proposals for avoidance algorithms and sensor layouts, but adapting these systems to certain UAV characteristics and keeping the cost low continues to be a challenge. Therefore, the main goal of this work is to improve the safety on low-cost fixed-wing mini UAVs regarding the detection of obstacles during their flight. It is part of an extensive obstacle detection and collision avoidance system, represent-

ing a two-stage "sense" and "avoid" problem, being this work focused solely on the former.

2. Benchmark of Sensors

A thorough study was conducted on the various types of sensors available on the market that could be integrated into our UAV. After this analysis, one of each sensor type was picked to be compared to the others, regarding their range and field of view (FOV), so that their attributes and flaws could be better showcased. The picked sensors for this comparison were the uAvionix pingRX ADS-B [4], the Lightware LW20/C laser rangefinder [5], the Aerotenna μ Sharp Patch RADAR [6], the Intel D435 stereo camera [7] and the MaxBotix MB1242 sonar [8]. All these sensors' sensed areas on the horizontal plane are represented in Figure 2, except for the ADS-B sensor, due to its omnidirectionality and the fact that its range depends on the power of the other aircraft's emitted signal. The sonar's FOV is almost invisible as a result of its small range (two orders of magnitude below the RADAR's range).

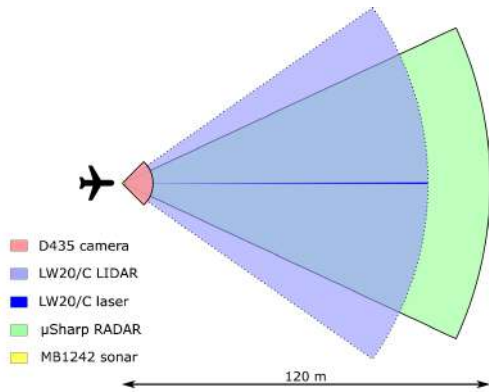


Figure 2: Comparison of several sensors' ranges and FOVs

It is important to note that the LIDAR, due to its multidirectionality, can scan with different angular apertures and its area is only limited by the used scanning servo. In Figure 2, an arbitrary 70° horizontal FOV was chosen and, because of this, the limits of the sensed area were dotted. The LW20/C's area, when the scanning mode is not activated, is represented in dark blue, where its 0.3° beam divergence can be observed.

The camera's sensed area is associated with its depth image sensors. The infra-red and color cameras have their own range and FOV but these are more applicable to complement other sensors as they do not provide depth data.

Based on this comparison, the ultrasound and stereo vision sensors were not modeled in section

3 due to their small range, as identifying obstacles when they are only at a distance of 10 m or 0.765 m, when the UAV is traveling at a maximum cruise speed of 15 m/s, generally, does not result in successful avoidance maneuvers. The ADS-B was also excluded for being a cooperative sensor, meaning it would require other vehicles to be equipped with similar equipment to allow the UAV to detect them, which is outside the scope of this work.

3. Sensor Models

A sensor model is an abstraction of the actual sensing process that describes the information a sensor can provide, how this information is limited by the environment and how it can be enhanced by data obtained from other sensors.

For the developed simulations, different sensors need to be modeled in order to compare their behavior and find the combination of sensors that achieve the best results. The sensors are characterized by their range, FOV, accuracy and data acquisition frequency. The values used for these parameters are from the sensors presented in section 2, which were obtained from their technical manuals or inferred from available data. The considered parameters are presented in Table 1.

Table 1: Characteristics of the different sensors used in simulations

	LIDAR	Laser rangefinder	RADAR
Range (m)	100	100	120
Horizontal FOV ($^\circ$)	variable	0.3	50
Accuracy (m)	0.2	0.2	0.22
Maximum Frequency (Hz)	388	388	90

3.1. LIDAR/Laser Rangefinder Model

Fayad and Cherfaoui [9] presented an approach to solve the problem of tracking partially hidden objects by a single layer laser scanner to be used in driving situations. In the proposed method, if an object is totally visible, it is considered that its half was detected and the remaining of the obstacle is reconstructed assuming symmetry, where the center of symmetry is the medium point of the segment connecting the first and last point of the cluster. In our simulations, the obstacles were modeled as circles, so this distance corresponds to the diameter of the obstacle.

This reference also provides a solution to the errors caused by the higher distance between consecutive points in farther obstacles which results in smaller detected dimensions, as seen in Figure 3, where the modeled obstacle is considerably smaller than the real obstacle.

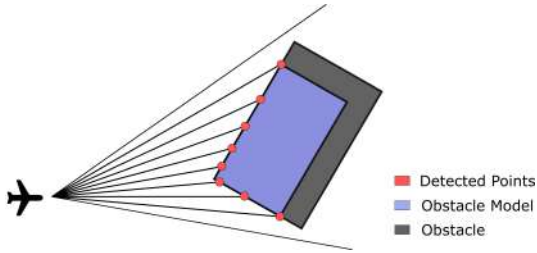


Figure 3: Obstacle reconstruction using a LIDAR

To solve this problem, the measured diameter is passed through the time filter

$$D_k = D_{k-1} + G(D_{meas} - D_{k-1}), \quad (1)$$

where G ($0 < G < 1$) is the filter gain, D_k is the filtered diameter at instant t_k , D_{k-1} is the filtered diameter at instant t_{k-1} , and D_{meas} is the measured dimension at instant t_k .

The gain needs to be carefully selected as it impacts the speed of the variation of the dimensions. A small gain corresponds to a slow variation and it is preferable for noisy environments but not suitable for high relative speed objects. The gain can be determined by

$$G = 1 - \sqrt[n]{1 - p}, \quad (2)$$

where p corresponds to a fraction that represents the desired accuracy of the dimensions and n corresponds to the number of filter cycles required to get an accuracy of p .

Regarding the tracking phase, classical Kalman filters [10] were used, where the motion of detected obstacles is considered to be two-dimensional, linear and constant between consecutive scans. This simplification describes the state of the targets with an acceptable error, considering a high scanning frequency. This model assumes a LIDAR that only scans horizontally, but if the rangefinder was to be attached to a gimbal with two degrees of freedom, it would have to be extended to include the third dimension.

3.2. RADAR model

To evaluate the system performance, the RADAR sensor was modeled in the context of the Sense and Avoid system. So, this model addresses the angular accuracy, update rate, range and field of view of the RADAR, rather than being a lower-level model that would deal with signal and environment modeling.

Assuming the RADAR sensor outputs the range, bearing and elevation of the detected obstacles, the state estimation becomes more complicated than the estimations used in the previous model, as these outputs are polar, whereas the intruder dynamics are best expressed in rectangular coordinates.

Therefore, the chosen radar model was the converted measurement Kalman filter (CMKF) due to its easier implementation [11]. Once again, for simplicity's sake, all the following equations reflect a two-dimensional model that can easily be extended to 3-D.

The unbiased conversion [12] was used, as the standard conversion method gives biased inconsistent estimates for certain levels of cross-range measurement error owing to the nonlinear transformation of the noisy bearing. Using the unbiased conversion, considering the measurement errors are modeled as Gaussian white noise, the compensation of the bias is multiplicative and the conversion is given by

$$x_m^u = \lambda_\alpha^{-1} r_m \cos(\alpha_m) \quad (3)$$

$$y_m^u = \lambda_\alpha^{-1} r_m \sin(\alpha_m). \quad (4)$$

where (x_m^u, y_m^u) are the measurements converted to the Cartesian frame, r_m is the measured range, α_m is the measured azimuth and λ_α is the bias compensation factor given by

$$\lambda_\alpha = e^{-\sigma_\alpha^2/2}, \quad (5)$$

where σ_α is the standard deviation of the noise in the azimuth measurements.

Finally, the covariance matrix to be used in the Kalman Filter is given by

$$\mathbf{R}_u = \begin{bmatrix} \text{var}(x_m^u | r_m, \alpha_m) & \text{cov}(x_m^u, y_m^u | r_m, \alpha_m) \\ \text{cov}(x_m^u, y_m^u | r_m, \alpha_m) & \text{var}(y_m^u | r_m, \alpha_m) \end{bmatrix}. \quad (6)$$

The computation of these variances are not included here, but can be seen in reference [12].

4. Multisensor Data Fusion

When the sensing system is composed of multiple sensors, the input data from the sensors needs to be merged in some way. For this work, the weighted filter method [13] was used. In this approach, a weight is computed for each of the sensors, which represents its reliability. Having computed all the sensor weights, the sensor with the best result is picked to provide the measurements in the present iteration of the process.

To compute the weights, the UAV needs to be also equipped with reference data sensors, which provide information about the UAV's state. IMUs and optical flow sensors are examples of reference data sensors used to evaluate the reliability of the main sensor data and help to decide between those sensors, based on the rationale that changes in distance to obstacles correspond to analogous changes in the UAV's position. If the obstacles are stationary, these variations should coincide. If the ob-

stacles are moving, this information becomes corrupted, but it is unlikely that this motion corresponds better to randomly wrong measurements.

The weights are computed by comparing all possible sensor combinations of main data and reference data using a differential norm, where the obstacle distance corresponding to the sensor with the lowest weight is considered the final result, while the remaining are rejected based on the idea that they are corrupted. However, if the computed weights have a low variation, the sensor values are fused according to their weights.

5. Obstacle Detection and Avoidance Algorithms

In this section, the chosen collision detection and avoidance algorithms based on the work developed in reference [14] are explained in detail. All subsequent simulations make use of the system described here.

In the developed algorithm, each detected obstacle has several safety zones associated with it, which play a role in the collision detection phase as well as in the avoidance phase. The obstacles were modeled as spheres and, as such, the collision radius (R_c) defines the volume of the obstacle and a collision is said to occur if this radius is trespassed. The safety radius (R_s) defines the minimum distance that should be maintained between the UAV and the obstacle to take into account possible deviations and uncertainties that could happen during the detection and path prediction phases. The action radius (R_a) is the distance from which the replanned paths begins to depart from the original path given by the global planner. Lastly, the detection radius (R_d) represents the distance from which an obstacle is considered by this algorithm. The R_s should be similar to the UAV's size; the R_a should be comparable to the R_s and the R_d corresponds to the range of the sensors used. A representation of the described safety zones are displayed in Figure 4.

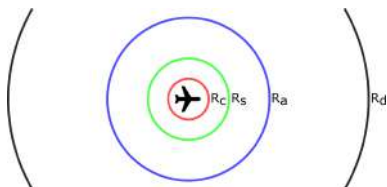


Figure 4: Representation of the safety zones around an obstacle

5.1. Geometric Collision Detection Method

The chosen collision detection method computes straight projections of the obstacles, considering future distances between the obstacles and the UAV. As such, the resulting collision detection method

consists on computing the closest point of approach (CPA) between the UAV and the target, assuming that both vehicles will maintain constant velocities and rectilinear paths. If this distance is smaller than the safety radius, an evasive maneuver must be performed, otherwise the obstacle is not considered a threat to the UAV. In case of multiple collisions being detected, the obstacles are sorted according to their times for collision t_{CPA} , so that the obstacles associated with possible collisions that would happen first are avoided before the remaining ones.

5.2. Potential Fields Method

To solve the local path planning problem, the Potential Fields approach is used, where the waypoints and obstacles are considered charged particles. Considering this analogy, the waypoints generate an attractive field, the obstacles a repulsive field and the sum of all forces is used to generate the direction of motion.

The attractive potential is given by

$$\mathbf{f}_{at} = \alpha_{PF} \frac{P_c - P}{\|P_c - P\|} + (1 - \alpha_{PF}) \frac{P_n - P_c}{\|P_n - P_c\|}, \quad (7)$$

where the first term is responsible for guiding the UAV to the nearest point of the global path and the second term is responsible for guiding the UAV to the next defined waypoint. P is the the UAV's position, P_c is the closest point of the global path and P_n is the position of the next waypoint. α_{PF} is responsible for giving more or less predominance to each term.

An example of a global path to a waypoint and its corresponding attractive potential field is represented in Figure 5 for $\alpha_{PF} = 0.7$.

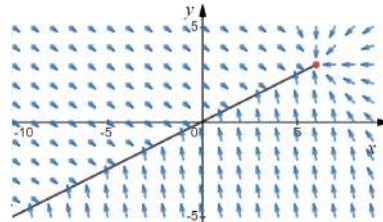


Figure 5: Attractive field for a linear path with $\alpha_{PF}=0.7$

Using a simple repulsive potential to avoid obstacles is not feasible since that would lead to irregular motion around the obstacle. So instead, the potential associated to the obstacle is described by

$$\mathbf{f}_{rep} = \begin{cases} \infty \frac{\mathbf{d}_0}{\|\mathbf{d}_0\|} & , \text{ if } \|\mathbf{d}_0\| \leq R_c \\ S_m \mathbf{s} & , \text{ if } R_c < \|\mathbf{d}_0\| \leq R_s \\ S_m \frac{R_a - \|\mathbf{d}_0\|}{R_a - R_s} \mathbf{s} & , \text{ if } R_s < \|\mathbf{d}_0\| \leq R_a \\ 0 & , \text{ if } \|\mathbf{d}_0\| \geq R_a \vee \theta \leq \theta_c \end{cases} \quad (8)$$

This way, the field is different according to the distance between the obstacle and the UAV. If the UAV is in the collision zone, the field will be repulsive (\mathbf{d}_0 is the vector pointing from the obstacle to the UAV) with infinite intensity. If it is in the safety zone, the field will have the direction of \mathbf{s} , a swirling term that makes the UAV maneuver in the correct direction, and the intensity of S_m , a constant to be defined depending on the velocity of the UAV. In the action zone, the field is similar to the previous one but with the addition of a gradient term that ensures the intensity of the field decreases linearly with the distance of the UAV to the obstacle until becoming null for $\|\mathbf{d}_0\| = R_a$. Lastly, outside the action zone, the obstacle has no influence in the motion of the UAV, thus the field intensity is null. To avoid the UAV being trapped around the obstacle, the generated field needs to become zero once the obstacle is overcome. To achieve this, the angle θ between the desired direction of motion and the direction of the obstacle is also computed and the field becomes null if θ is smaller than a defined cut-off angle θ_c . A potential field associated with an obstacle is displayed in Figure 6.

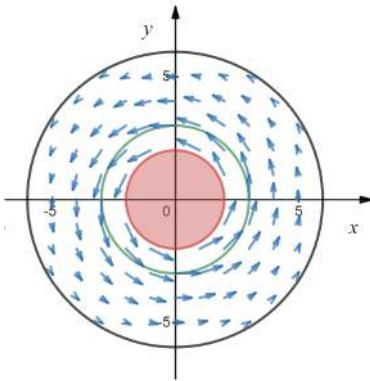


Figure 6: Repulsive field for an obstacle with $R_c = 2$, $R_s = 3$ and $R_a = 6$

6. Definition of UAV's Model

Before performing the necessary simulations, several parameters associated with the UAV's dynamics and the Kalman tracking need to be carefully determined, namely the UAV's speed, maximum angular velocity and its measurement error covariance matrix.

6.1. UAV's Speed and Angular Velocity

Since the simulations were performed in a two-dimensional environment, the two most important performance parameters to define are the UAV's speed (V) and the maximum angular velocity (ω) of its turns.

Considering the example of the Tekever AR4 described in section 1, the UAV is considered to travel with a speed between 8 m/s and 15 m/s. The faster the UAV moves, the larger its angular velocity needs to be so that the obstacles can be effectively avoided. To prove this concept and to get the lowest maximum angular velocity needed for different possible UAV speed values, a series of simulations were performed. In these simulations, the UAV was set in a head-on collision course with an obstacle with a 2 m radius and a safety radius of 2 m. The obstacle approaches with the same speed as the UAV, which is equipped with a RADAR with a 50° FOV and a 120 m range. For each of the tested speeds, the maximum angular velocity was decreased until the UAV could not perform the avoidance maneuver without breaching the safety zone around the UAV. The results obtained from these tests are presented in Figure 7, in which a linear dependency can be recognized.

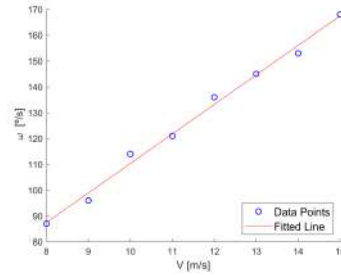


Figure 7: Angular velocity needed to avoid obstacle safely for different speeds

To check the validity of these results, the avoidance maneuvers can be approximated to coordinate turns [15]. A coordinate turn is a turning maneuver made at a vertical and constant angular velocity and in which the lateral component of the resulting force is null. Considering that there is no wind, the slip is almost null and the angle of attack and climb angle are very small, the speed and the angular velocity are related by

$$\tan(\phi) = \frac{\omega V}{g}, \quad (9)$$

where ϕ is the correspondent roll angle and g is the standard acceleration due to gravity ($\approx 9.81 \text{ m/s}^2$).

The avoidance maneuver is not performed at a constant angular velocity, but this approximation can be made to check the roll angles corresponding

to the speeds and angular velocities obtained. Some of the obtained values are displayed in the Table 2.

Table 2: Roll angles for each maneuver considering the performance of a coordinate turn

V (m/s)	ω ($^{\circ}$ /s)	Roll Angle ($^{\circ}$)
8	87	51.1
10	114	63.8
12	136	71.0
15	168	77.4

The obtained roll angles are acceptable considering the urgency of the maneuvers needed to avoid obstacles. For the highest speed of 15 m/s, the corresponding roll angle is already pretty high but achievable nonetheless. So, for the next simulations, the maximum angular velocity of the turns was set to 168 $^{\circ}$ /s.

6.2. Measurement Error Covariance Matrices

As described in section 3, using polar measurements and a Cartesian state space leads to inaccuracies when tracking the obstacles with a Kalman filter. To test the measurement error covariance matrix described in that section, the UAV was put in a head-on collision course, where the UAV is moving at 8 m/s and obstacle is moving at 10 m/s. The UAV was equipped with a RADAR with the specifications of the Aerotenna μ Sharp Patch (100 m range, 50 $^{\circ}$ FOV and 0.22 m accuracy). The noise was divided into a radial and an angular component, where both components were modeled as a zero-mean Gaussian noise, with the corresponding variance chosen so that 99.73% of the set would be within the accuracy range. The angular accuracy was considered at half the sensor range (50 m).

To perform this test, one hundred simulations were performed for the unbiased conversion matrix, the standard conversion matrix and the identity matrix (as a control group). Then, the average position errors were computed for both Cartesian coordinates. The root mean square (RMS) deviation for the three matrices and for both coordinates is represented in Table 3. Only the first 250 scans were considered in the computations, so that the points where the obstacle is not detected anymore do not influence this metric, as the avoidance maneuver starts after this point.

From Table 3, one can conclude that using the standard conversion or the unbiased conversion result in very similar results. This may be due to the particular conditions of our study, where the sensor range and the noise variance are not very high. In spite of the similar results, the unbiased conversion matrix will be used in all the following simulations.

Table 3: Root mean square deviations for each of the used matrices

RMS [m]	x axis	y axis
Standard conversion matrix	0.0165	0.0013
Unbiased conversion matrix	0.0163	0.0016
Identity matrix	0.5993	0.0009

7. Sensor Parametric Studies

In this section, a study of the response of the UAV to imminent collisions, when it is equipped with sensors with different parameters is made, to verify if the chosen sensors perform acceptably in avoiding incoming obstacles.

7.1. Varying Range Simulations

To study how the sensor's range influences the response of the UAV to detected obstacles, the UAV was set in a head-on collision course with an obstacle with a radius of 2 m, a safety radius of 4 m and animated with a speed of 10 m/s. The UAV is equipped with a RADAR sensor with a FOV of 50 $^{\circ}$ but, for this kind of experience, the type of sensor used does not affect the results much. In Figure 8, the different trajectories from UAVs animated with a speed of 8 m/s with RADARs with varied ranges are presented.

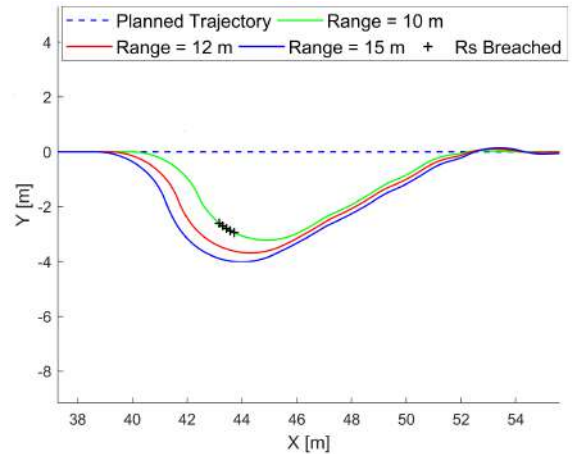


Figure 8: Avoidance trajectories for UAVs equipped with a RADAR with different ranges for a head-on collision threat

The UAV behaves very similarly for all illustrated cases. The obstacle is always properly tracked and avoided, which results in similar tight maneuvers. If the UAV is equipped with a RADAR with a range of 10 m, the UAV is already inside the action radius of the obstacle when the obstacle is detected. Because of this, the UAV immediately initiates the avoidance maneuver but cannot avoid breaching the

safety radius of the obstacle. For this example, ranges greater than 15 m result in identical trajectories.

7.2. Varying Field of View Simulations

To test the effect of the FOV of the sensor on the avoidance capabilities of the UAV, the UAV was set in a 30° angled collision course with an obstacle moving at a speed of 10 m/s, while being equipped with a LIDAR that performs a measurement every half degree with a range of 100 m. The LIDAR gain from equation (2) also needs to be defined. For the sensor to reach 99% of the real dimensions, p is set to 0.99 and, to get this precision before the obstacle transverses 10% of the 100 m range, the filter needs to perform 20 iterations (n), considering the LIDAR is working at a 50 Hz frequency and assuming the obstacles can move at the same speed of the UAV, which results in a maximum relative speed of 30 m/s. Knowing n and p , the minimum gain to be used can be computed using said equation, it being 0.2057. The responses of the UAV for different FOVs, when it is moving at a speed of 8 m/s, is displayed in Figure 9.

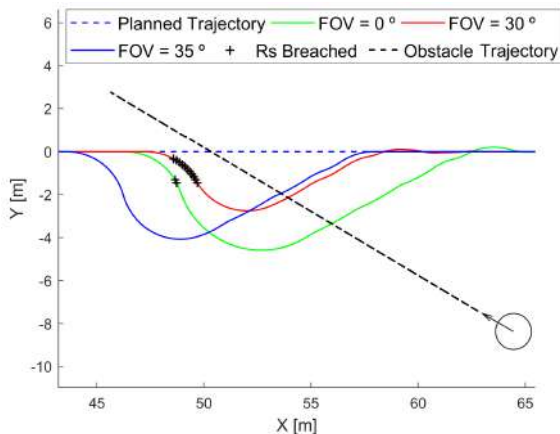


Figure 9: Avoidance trajectories for UAVs equipped with a LIDAR with different FOVs for an angled collision threat

For a FOV of 30° , the obstacle is detected when it is already dangerously close to the UAV so the UAV breaches the safety radius for several points, despite avoiding a collision. For FOVs greater than 35° , the obstacle is properly tracked in advance, which results in a proper safe maneuver. Finally, for a FOV of 0° , which corresponds to a fixed laser rangefinder, the UAV detects the obstacle only when it is directly in front of it, which causes a quick breach of the safety radius. Because of the singular nature of this case, the obstacle's velocity can only be tracked with a radial component and so, the obstacle is tracked as being in a head-on collision course with a small velocity. This leads to a wide maneu-

ver which results in the UAV leaving the obstacle's safety radius after only a couple points.

The obstacles were avoided by the UAVs with different sensors, but the success of the maneuver depends on the approach angle of the obstacle. Small FOVs also result in inadequate velocity tracking, which cause the UAV to unreasonably distance itself from the planned trajectory.

8. Optimal Sensing System

In this section, an optimization study was made in order to find the best sensor configuration, for different sensor sets.

Firstly, fifty scenarios were randomly generated, where each scenario leads to imminent collisions. Then, a function $f(\beta)$, to be minimized and dependent on the sensor orientation β , was created. $f(\beta)$ was initialized to null and all the generated scenarios were run, where, for each instant, $f(\beta)$ was incremented by

$$\begin{cases} f(\beta) = f(\beta) + 50 & , \text{ if } \|\mathbf{d}_0\| \leq R_c \\ f(\beta) = f(\beta) + 1 & , \text{ if } R_c < \|\mathbf{d}_0\| \leq R_s \end{cases}, \quad (10)$$

where R_c is the collision radius, R_s is the safety radius and $\|\mathbf{d}_0\|$ is the distance between the UAV and a given obstacle. After running all the scenarios, the cumulative value of $f(\beta)$ can be evaluated: the lower its value, the less failures and close-calls happened.

To minimize this function, the Genetic Algorithm (GA) [16] was used. This method is a gradient-free, population-based method, which, instead of working with a single solution candidate, deals with a set of solutions that are updated simultaneously from iteration to iteration, which increases the likelihood of finding the global optimum. In GA, the design point associated with an individual is represented as a chromosome. At each generation, the chromosomes of the fitter individuals are passed on to the next generations after undergoing the genetic operations of crossover and mutation. New candidates for the solution are generated with a mechanism called crossover which combines part of the genetic patrimony of each parent and then applies a random mutation. If the new individual, called child, inherits good characteristics from his parents, it will have a higher probability of survival. In the context of genetic algorithms, the value of the objective function is termed the fitness and the variables need to be bounded. The problem can then be posed in standard form as

$$\begin{aligned} & \text{Minimize} && f(\beta) \\ & \text{w.r.t.} && \beta, \\ & \text{subject to} && lb < \beta < ub, \end{aligned} \quad (11)$$

where lb and ub are the lower and upper bounds of β , respectively, to be defined for each particular case.

Before performing the simulations, several optimization parameters needed to be defined:

- The initial population was set to be created with a uniform distribution;
- The crossover function was set to create 80% of the population in each generation;
- Because the variables are bounded, the mutation function randomly generates directions that are adaptive with respect to the last successful or unsuccessful generation, where the chosen direction and step length satisfy the set bounds;
- The algorithm was set to stop after 20 generations, enough for one bounded variable to converge until the genetic diversity is very small;
- The population size was set to 30, enough to find the global minima in a timely manner.

These parameters were chosen following best practices [17].

8.1. Set of two RADARS

For a set of two RADARs, the orientation of each sensor was bounded between 0° and 90° from the longitudinal axis, in the horizontal plane and, to simplify the problem in order to reduce the computation time, the two RADARs were considered to have a symmetrical orientation about the UAV's longitudinal axis, which is an acceptable approximation. This way, the algorithm only had one variable to optimize.

The algorithm performed well and, when the optimization was halted, the best fitness was 746 for an orientation of 34.6° , as seen in Figure 10. The expected result of this simulation was for the sensor orientation to be close to 25° , which would yield the same result as if the UAV was equipped with a RADAR sensor with a doubled FOV.

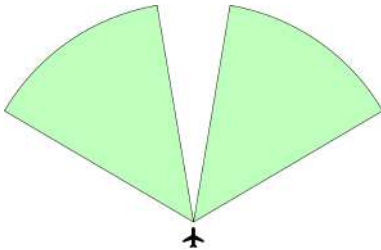


Figure 10: Optimal configuration for two RADARs

A comparison of performance between the optimal orientation, a 25° orientation and a single

RADAR pointing forward is presented in Table 4, where a failure happens when the UAV collides with an obstacle and a close call happens if the UAV breaches the safety radius of an obstacle.

Table 4: Comparison of performance for different orientations for two RADARs

Orientation	Fitness Value	Failure Rate	Close Call Rate
0°	1625	8%	22%
25°	1051	6%	26%
34.6°	746	6%	20%

All of the failures that occur when the UAV is equipped with one RADAR pointing forward do not happen for the optimal solution because, in those cases, obstacles would approach the UAV from an angle that would not allow their detection by a single RADAR. However, because the optimal solution cannot detect obstacles directly in front of the UAV, two scenarios that were successes for one RADAR become failures but, because the random scenarios include a larger number of obstacles approaching from a wide angle than approaching head-on, the optimal solution corresponds to an angle larger than 25° . Moreover, overlapping FOVs would result in the use of the weighted filter data fusion technique and, consequently, more accurate measurements, but obstacles approaching from wider angles would not be detected.

8.2. Set of two Laser Rangefinders

Like in the previous optimization, in this one the two sensors were considered to be symmetrical about the UAV's longitudinal axis, so that only one variable bounded between 0° and 90° needed to be optimized. After 20 generations, both the best fitness and the mean fitness were 348 for an orientation of 25.1° (Figure 11).

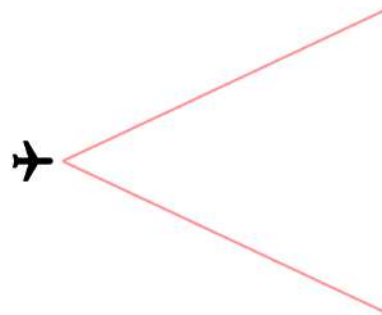


Figure 11: Optimal configuration for two laser rangefinders

As seen in Table 5, the optimal configuration results in no collisions in all scenarios.

Table 5: Comparison of performance for different orientations for two laser rangefinders

Orientation	Fitness Value	Failure Rate	Close Call Rate
0°	1753	12%	40%
25.1°	348	0%	44%

The optimal solution results in a much lower fitness value than when only one laser rangefinder pointing forward is used, as obstacles coming from an angled approach can be detected before the collision. However, despite the zero collisions, in 44% of the scenarios, the safety radius of obstacles were breached because when collisions with moving objects are imminent, a UAV equipped only with laser rangefinders is not capable of properly tracking the obstacles.

8.3. Set of two Laser Rangefinders and one RADAR
This optimization involved three sensors: one fixed radar pointing forward and two laser rangefinders symmetrical about the UAV’s longitudinal axis, whose orientation was bonded between 0° and 90°. When the algorithm halted, the best fitness was 304 for an orientation of 69.2° (Figure 12).

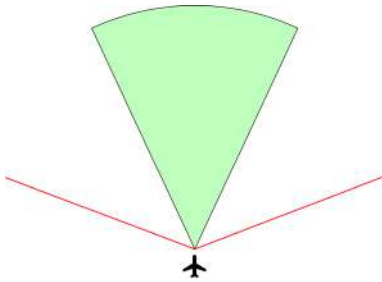


Figure 12: Optimal configuration for two laser rangefinders and one RADAR

In Table 6, the performance of the optimal solution is compared to the performance of the solutions that would result from a UAV being equipped with only one type of sensor, it being a RADAR pointing forward or two symmetrical laser rangefinders with an orientation of 69.2°.

Table 6: Comparison of performance for the optimal solution when using different sensors

Sensors	Fitness Value	Failure Rate	Close Call Rate
One RADAR	1625	8%	22%
Two lasers	1660	8%	62%
One RADAR and two lasers	304	2%	18%

Despite the two lasers configuration and the one RADAR configuration having very similar fitness values, a UAV with only two lasers has almost the triple of close calls than a UAV with one RADAR

because the UAV will only be able to detect most of the obstacles when the safety radius is already breached. By contrast, the optimal solution results in only one failure and a reduced number of close calls.

The obtained solution was expected because obstacles approaching in a head-on collision course could be detected by the RADAR, while the ones approaching in an angled collision course could be detected by the heavily displaced laser rangefinders. Once again, the optimal solution did not involve overlapping sensors, which would increase the accuracy of the measurements through the use of the chosen data fusion algorithm, but would not allow the detection of obstacles approaching from a wider angle, which is more favorable.

9. Conclusions

9.1. Achievements

This work was developed with the goal of enhancing the safety in the flight of fixed-wing mini UAVs, in regard to the detection of obstacles during flight. The focus was on the first stage of the S&A phase, responsible for the acquisition of the necessary information that allows the vehicle to detect threatening situations like proximity to sensitive infrastructures and route of collision with other manned or unmanned aircraft.

Several possible sensors were considered to be used by the developed system and after making a market study on available sensors to know which sensors had the most adequate attributes (range, FOV, accuracy, cost), ultrasound and stereo vision sensors were rejected due to the small range they provided, ADS-B sensors were rejected for only detecting other aircraft when they were also equipped with this cooperative sensor, which would not fit the scope of this work, despite existing small models that could be implemented in mini UAVs.

This work was part of a comprehensive obstacle detection and collision avoidance system, so an in-depth description of the potential field approach, the chosen algorithm, was also made.

To integrate the adequate sensors into the avoidance system already developed, they needed to be modeled. These models took into consideration the range, FOV and accuracy that the real sensors were characterized by. For laser rangefinders and LIDARs, classic Kalman filters were sufficient to guarantee adequate tracking. However, for the RADAR sensors, a Converted Measurement Kalman Filter with unbiased conversion was required, due to the conversion of the measurements from polar to Cartesian coordinates. Additionally, to fuse the data obtained from different redundant sensors at a decision level, the weighted filter technique was selected due to its simplicity and effectiveness.

Having modeled the sensors, several parametric studies were made, where the impact of the range and field of view of the vehicle in the avoidance of obstacles from predetermined scenarios was made clear. From these simulations, the specifications of the studied sensors were verified as more than acceptable for avoiding obstacles at the considered speed range. Additionally, an optimization study was conducted to determine the best orientation that the sensors should have when the UAV is equipped with different sets of sensors. The optimization process was accomplished by using the genetic algorithm to minimize a function closely associated with the success and failure of the avoidance maneuvers. Because the sensors in the tested sets were redundant, none of the optimal solutions involved using the selected sensor fusion method, as having the sensors pointing at different directions is more valuable than having them pointing at the same obstacle and fusing the results.

Overall, the developed system provided a satisfactory solution to the obstacle detection problem of mini UAVs in a simulated environment.


9.2. Future Work

There are several improvements and future work that can be made. The simulations can be adapted to a space that better integrates the vehicle dynamics, so that the used models better reflect the reality. This new simulated environment should also be able to generate more complex obstacles that better reflect the diversity found in the real world. A study can also be made regarding the fusion of range sensors with image sensors, since this work only dealt with the fusion of redundant sensors.

Ground and flight tests should also be made to test how a vehicle would behave when using the chosen avoidance algorithm with different sensor configurations in the real world.

Finally, this work was developed with the objective of increasing the UAV's autonomy, but interaction with the operator should also be considered, so that more suitable decision systems can be developed.

References

- [1] P. Finnegan. *2019 World Civil Unmanned Aerial Systems Market Profile & Forecast*. Teal Group Corporation, August 2019.
- [2] K. Dalamagkidis. Classification of UAVs. In K. P. Valavanis and G. J. Vachtsevanos, editors, *Handbook of Unmanned Aerial Vehicles*, pages 83–91. Springer Netherlands, 2015. doi: 10.1007/978-90-481-9707-1_94.
- [3] TEKEVER AR4. <http://uas.tekever.com/ar4-evo/>. Accessed: 24-11-2020.
- [4] *PING-RX ADS-B Dual Receiver*. uAvionix, 2019.
- [5] *LW20 / SF20 LiDAR sensor Product manual*. Lightware, 2018. Rev 9.
- [6] *μSharp Patch Collision Avoidance Radar*. Aerotenna, 2018.
- [7] *Intel RealSense™ D400 Series (DS5) Product Family*. Intel, 2018. Rev 001.
- [8] *MB1242 Datasheet*. MaxBotix, 2012.
- [9] F. Fayad and V. Cherfaoui. Tracking objects using a laser scanner in driving situation based on modeling target shape. In *2007 IEEE Intelligent Vehicles Symposium*, pages 44–49, June 2007. doi: 10.1109/IVS.2007.4290089.
- [10] M. S. Grewal, A. P. Andrews, and C. G. Bartone. Kalman filtering. pages 355–417. Wiley Telecom, 2020.
- [11] D. Lerro and Y. Bar-Shalom. Tracking with de-biased consistent converted measurements versus EKF. *IEEE Transactions on Aerospace and Electronic Systems*, 29(3):1015–1022, July 1993. doi: 10.1109/7.220948.
- [12] M. Longbin, S. Xiaoquan, Z. Yiyu, S. Z. Kang, and Y. Bar-Shalom. Unbiased converted measurements for tracking. *IEEE Transactions on Aerospace and Electronic Systems*, 34(3):1023–1027, 1998. doi: 10.1109/7.705921.
- [13] N. Gageik, P. Benz, and S. Montenegro. Obstacle detection and collision avoidance for a UAV with complementary low-cost sensors. *IEEE Access*, 3:599–609, May 2015. doi: 10.1109/ACCESS.2015.2432455.
- [14] J. Alves. Path planning and collision avoidance algorithms for small RPAS. Master's thesis, Instituto Superior Técnico, June 2017.
- [15] B. Etkin and L. D. Reid. *Dynamics of flight*, volume 2. 3rd edition, 1959.
- [16] M. J. Kochenderfer and T. A. Wheeler. *Algorithms for optimization*. Mit Press, 2019. ISBN:9780262039420.
- [17] Mathworks . Global optimization toolbox™: User's guide (r2020b). https://www.mathworks.com/help/pdf_doc/gads/gads.pdf, 2020. Accessed: 29-12-2020.